International Journal of Coal Geology 275 (2023) 104314

Contents lists available at ScienceDirect

International Journal of Coal Geology

journal homepage: www.elsevier.com/locate/coal

Experimental study of the impact of CO_2 injection on the pore structure of coal: A case study from the Bowen Basin, Australia

Alireza Salmachi [a], Abbas Zeinijahromi [a], Mohammed Said Algarni [a], Nawaf Abdullah Abahussain [a], Saad Abdullah Alqahtani [a], Alexander Badalyan [a], Mohammad Rezaee [b], Mojtaba Rajabi [c,*]

[a] School of Chemical Engineering, University of Adelaide, Adelaide, SA 5005, Australia
[b] Department of Petroleum Engineering, Amirkabir University of Technology, Tehran, Iran
[c] School of the Environment, University of Queensland, St Lucia, QLD 4072, Australia

ARTICLE INFO

Keywords:
Carbon Capture and Storage
Permeability
Micro-CT scan imaging
Matrix swelling
Borehole image log

ABSTRACT

This study investigates the impact of carbon dioxide (CO_2) on the pore structure of coal during CO_2 injection to understand the technical challenges associated with CO_2 sequestration in depleted coal seam gas reservoirs. In an integrated approach, Micro-Computed Tomography (micro-CT) scanning, helium porosity and air permeability tests are performed on a coal sample prior to and after CO_2 flooding experiments to identify both reversible and irreversible changes in cleat and fracture networks. The results indicate that irreversible changes contribute to a 43% reduction in effective porosity, which can be readily observed in the 3D model of the cleat and fracture networks constructed after CO_2 flooding. At lower effective stresses, pore compressibility offsets the matrix swelling effect, resulting in improved permeability, which is beneficial for CO_2 injection. Additionally, the analysis of borehole image logs of the study well reveals that most fractures and cleats terminate within coal intervals, with very few fractures extending into adjacent strata that are siltstone and fine sandstone with very low permeability.

1. Introduction

Carbon Capture and Storage (CCS) in deep geological formations can potentially play a significant role in decarbonizing heavy industries. CCS is considered a potential pathway to achieving net-zero targets, particularly for industries where electrification is challenging and costly, such as the lime and cement industries (Hong, 2022; Jinlong and Liwen, 2020; Li et al., 2023; Shaw and Mukherjee, 2022).

Depleted hydrocarbon reservoirs, including depleted coal seam gas reservoirs and deep saline aquifers, are potential targets for CO_2 storage projects (Ali et al., 2022; Martin-Roberts et al., 2021). Coal seams, due to their large ratio of surface area to volume, offer up to seven times more potential CO_2 storage compared to other reservoirs (Hadi Mosleh et al., 2019). Additionally, the sequestration of CO_2 in coal seams can enhance the production of methane while simultaneously storing CO_2 in the coal matrix (Ferguson, 2008; Mukherjee and Misra, 2018; Wong, 2015).

Coal is classified as a dual-porosity porous medium, where its matrix primarily composed of micropores (i.e., <2 nm) and macropores (i.e., >50 nm) (Zhang et al., 2016). Gas storage in micro-porosity is controlled by the adsorption mechanism, while gas storage in macro-porosity, which mostly consists of interconnected cleats and natural fractures, is governed by compression (Harpalani and Chen, 1995; Qi et al., 2017; Salmachi and Haghighi, 2012; Zou et al., 2022). The cleat network (i.e., opening mode, sub-vertical natural fractures in coals) and natural fracture systems (i.e., any types of natural fractures that are not sub-vertical – or sinusoid fractures in vertical boreholes that penetrated into horizontal coal seams) predominantly control fluid flow within coal seams (Esen et al., 2020; Mukherjee et al., 2021).

Adsorption of gas in the coal matrix leads to an increase in matrix volume, known as matrix swelling, which subsequently decreases cleat/fracture aperture and volume (Mukherjee and Misra, 2018; Rogers et al., 2007; Su et al., 2019). Conversely, when gas is desorbed from coal matrix, it causes the matrix to shrink, resulting in an increase in pore volume (Clarkson and Salmachi, 2017; Mukherjee and Misra, 2018; Rogers et al., 2007; Su et al., 2019). The swelling of coal matrix can result in a reduction in porosity and permeability (Mazumder and Wolf,

* Corresponding author.
E-mail address: m.rajabi@uq.edu.au (M. Rajabi).

https://doi.org/10.1016/j.coal.2023.104314
Received 30 March 2023; Received in revised form 10 July 2023; Accepted 18 July 2023
Available online 22 July 2023

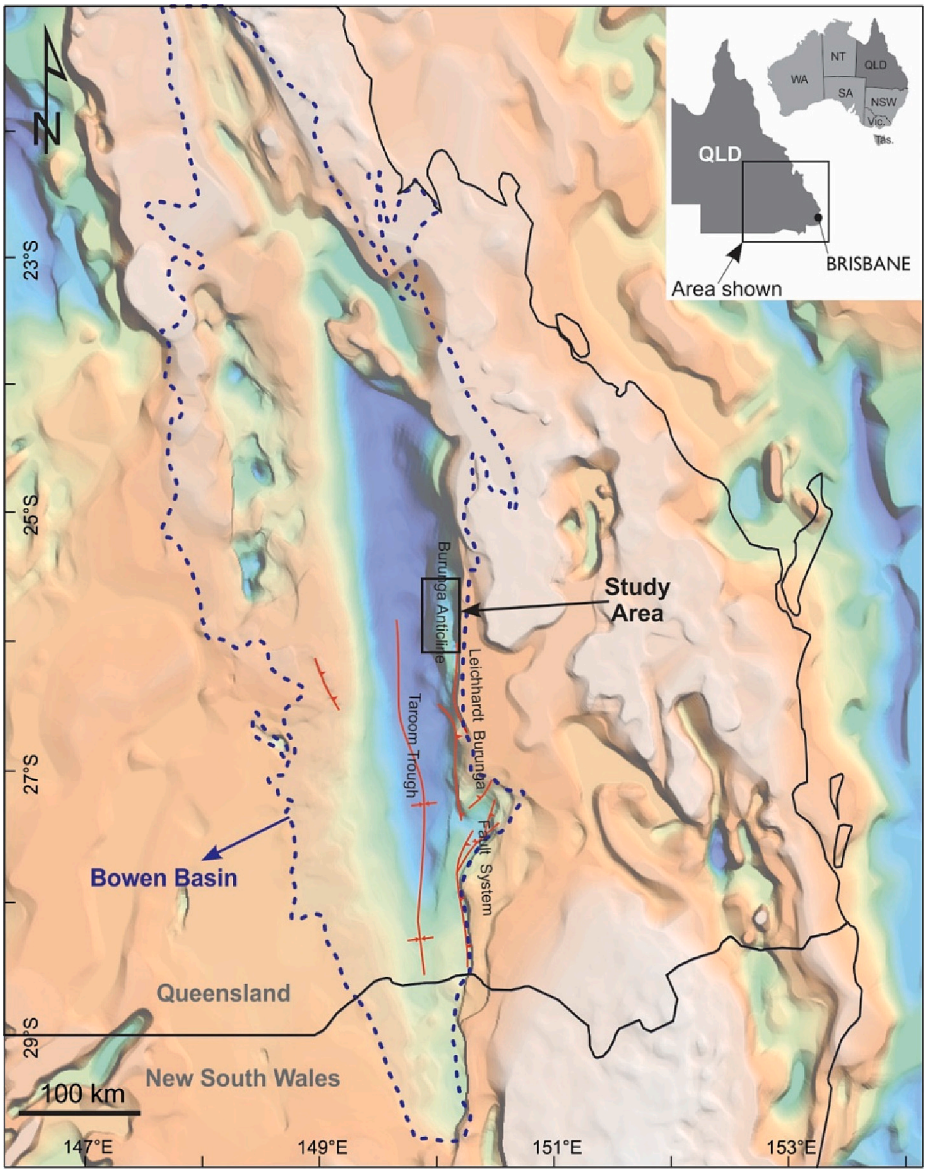

Fig. 1. Location of the study area (the Scotia Field) in the eastern side of the Bowen Basin. Major geological structures such as Burunga-Leichhardt fault system and Burunga anticline are also shown. The background image shows the depth to the basement in the region based on the basement map of Australia (FrOG-Tech, 2006).

2008). There are studies that have examined the effects of various parameters, including pressure, temperature, wettability, and coal rank, on CO_2 sequestration and coal swelling (Clarkson and Bustin, 2000; Day et al., 2008; Krooss et al., 2002; Li et al., 2010; Ranathunga et al., 2017). Matrix swelling due to CO_2 adsorption and the resulting decline in permeability have been documented in different basins (Fujioka et al., 2010; Gruszkiewicz et al., 2009; Majewska et al., 2009; Pan et al., 2010). Coal rank influences coal-CO_2 interactions (Li et al., 2022; Liu et al., 2020). High rank coals (e.g., anthracite) have a higher adsorption capacity because of their larger surface area, while medium rank coals tend to have a more developed cleat network and higher permeability (Ahamed et al., 2019; Du et al., 2021; Li et al., 2023). Therefore, measuring coal storability and injectivity for CO_2 are two important factors to consider for any CO_2 sequestration project.

Niu et al. (2019) discussed that coal matrix swelling can be attributed to solvent swelling effect, chemical reactions, and changes in surface energy. The dissolution of CO_2 in coal allows the macromolecular structure of the coal to relax and swell. CO_2 chemically reacts with compounds containing weakly polar or non-polar functional groups, resulting in the loosening of the coal by reducing its crosslinking degree. Moreover, CO_2 adsorption decreases surface energy in the coal matrix that leads to a reduction in mechanical properties of the coal including, compressive strength, elastic modulus, and tensile strength.

An early study reported an increase in the volume of coal blocks ranging from 0.2% to 1.6% at CO_2 pressures up to 15.2 MPa, indicating matrix swelling. However, the volume either declined or remained constant under pressures ranging from 15 to 71 MPa (Harpalani and Chen, 1995; Moffat and Weale, 1955). During CO_2 injection in coal, two opposing factors including matrix swelling and pore compressibility influence cleat aperture. During CO_2 injection, matrix swelling tends to reduce cleat aperture while pore compressibility tends to widen the cleats (Larsen et al., 1985). It should be noted that changes in cleat porosity because of coal swelling may increase the likelihood of cleat closure (Harpalani and Chen, 1995).

Coal permeability is a crucial parameter for evaluating CO_2 injectivity in coal seams. Effective stresses, porosity characteristics, temperature, fracture geometry, water content, coal type, and matrix swelling/shrinkage effects are the main factors that affect coal permeability (Gao et al., 2021; Han et al., 2022; Liu et al., 2017). Several laboratory measurements indicate that coal permeability decreases exponentially

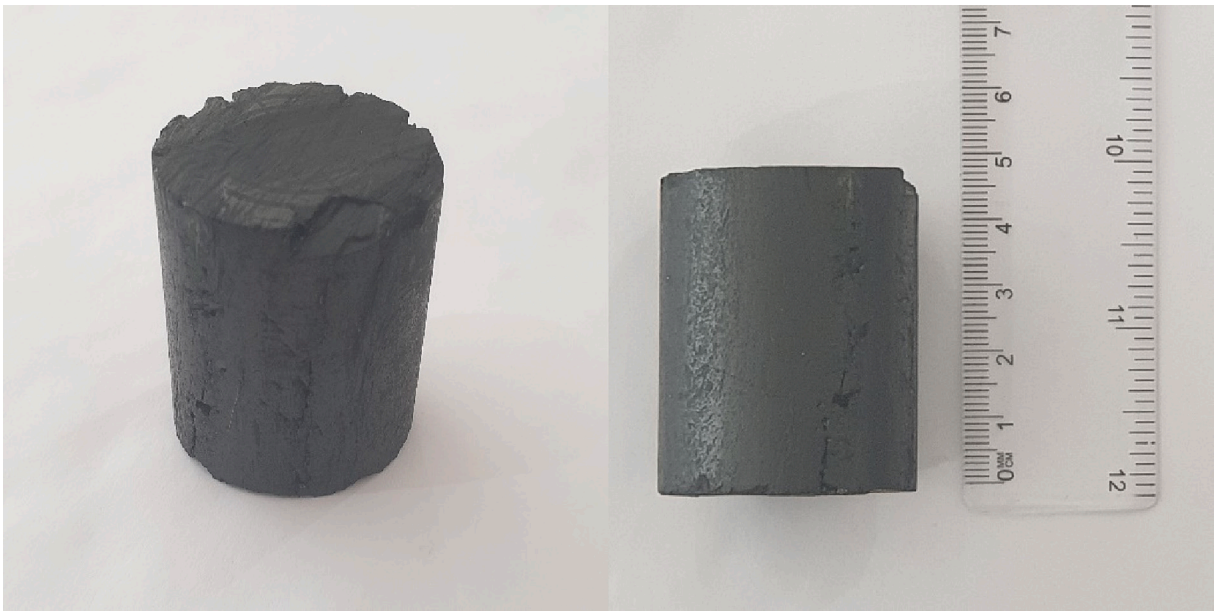

Fig. 2. The core plug used in experiments measures 47 mm in length and 34 mm in diameter. It was drilled parallel to the coal bedding and obtained from a core sample extracted from the study well.

as effective stress increases (Lin et al., 2020; Peng et al., 2014; Zhang et al., 2023). The behaviour of coal is not purely elastic when subjected to changes in effective stress. The stress loading path will continually evolves during the CO_2 sequestration process. Loading and unloading of the coal body can result in irreversible alternations in the mechanical properties of the solid matrix and cleat volume (Xin et al., 2021). Coal permeability hysteresis occurs during cyclic loading, and permeability cannot rebound to its pre-loading values. Therefore, studying permeability loss due to stress changes after CO_2 adsorption is necessary, as maintaining high CO_2 injection is crucial.

Experiments conducted by Bai et al. (2022) demonstarte that the reduction in coal permeability due to matrix swelling caused by CO_2 injection may be more significant than the increase in permeability resulting from matrix shrinkage during primary methane production. This is because coal exhibits a higher adsorption capacity toward CO_2 compared to CH_4. Furthermore, researchers have investigated the combined effect of in-situ effective stresses and matrix swelling on cleat clouser and permeability (Dong et al., 2021; Li et al., 2022). Chen et al. (2012) showed that under their experimental conditions, the swelling effect outweights compressibility, leading to a decline in permeability.

X-ray computed tomography technology is a non-destructive technique used to gain a deeper understanding and obtain accurate estimates of coal petrophysical properties (Fan et al., 2023; Jia et al., 2020; Mathews et al., 2017; Yarmohammadtooski et al., 2017). This technique employs X-ray technology and mathematical model algorithms to visualize cross-sections of samples and create 3D images for investigation of the pore structure of the cores. Subsequently, researchers employed this method to better understand CO_2 sequestration in coal seams, mineral dispersion, swelling/shrinking phenomena, and the effects of effective stress on coal microstructural properties (Wang et al., 2022; Wang et al., 2019; Yuan et al., 2022; Zhang et al., 2022).

There is a gap in the literature when it comes to quantifying both reversible and irreversible changes in pore structure of the coal during CO_2 flooding by different experimental techniques. Additionally, to the best of our knowledge, no previous work has examined the fracture network of coal and non-coal formations in the context of hydraulic communication between the reservoir and neighbouring strata during CO_2 injection. This study aims to address these gaps by quantifying both reversible and irreversible changes in pore structure of the coal during CO_2 injection through integrated CO_2 flooding experiments, micro-CT scan imaging, and porosity and permeability measurements. CO_2 and air flooding experiments are performed on a core sample using an in-house CO_2 flooding facility. High resolution 3D images of the core sample are constructed by micro-CT scan imaging before and after CO_2 flooding experiments to assess the extent of irreversible changes. Additionally, borehole image logs of the study well are analyzed to evaluate fracture intensity, dip, and their extension within both coal and non-coal intervals.

2. Geological setting and the study wellbore

The Bowen Basin, an Early Permian – Late Triassic basin in Australia, is known for its abundant thick coal seams and as a prolific source of coal and coal seam gas (Korsch and Totterdell, 2009a, 2009b; Salmachi et al., 2021).

This back-arc to foreland basin has undergone a complex structural and tectonic history that includes a series of subsidence, uplift, and closures (Baker et al., 1993; Korsch and Totterdell, 2009b; Totterdell et al., 2009). The basin initiated as a back arc basin during the Late Carboniferous and early Permian, which was followed by a phase of thermal subsidence in the early late Permian (Jell, 2013). A foreland basin with massive accumulation of coals were developed in the Late Permian that was later undergone significant compressive uplift and deformation during Middle and Late Triassic (Green et al., 1997; Korsch et al., 2009).

The core samples used in this study are obtained from a wellbore drilled in the Scotia Field, located on the eastern side of the Bowen Basin (see Fig. 1). This field is flanked by part of Burunga-Leichhardt fault system, and it produces gas from Late Permian Baralaba Coal Measures (equivalent to the Rangal and Bandana Coal Measures in north and southwest of the Bowen Basin) at depths of 700–1000 m. The Baralaba Coal Measures of the Burunga Anticline are highly fractured and display permeability suitable for commercial production. Full cores were extracted from Late Permian Baralaba Coal Measures including C2 (depth of 936 m to 970 m) and C3 (depth of 1035 m to 1039 m) seams for gas desorption and geomechanical tests. The rank of Baralaba coals in this area are around 0.55% to 0.7% Rv, with vitrinite content ~60% overall (high volatile bituminous coal) (Draper and Boreham, 2006). This study wellbore is vertical well that was completed as an open hole and has geophysical well logs such as the acoustic borehole image log,

Technical Data	
X-ray Source	40-100 kV, 20 W, <5 µm spot size at 4 W
X-ray Detector(s)	16 Megapixel sCMOS camera 4,096 x 4,096 pixels
Spatial Resolution	2.8 µm smallest pixel size, 6 µm details resolved with more than 10% contrast
Image Formats	Up to 7,800 x 7,800 x 2,500 pixels after a single scan
Scanning space	75 mm in diameter, up to 310 mm in length
Integrated Physiological monitoring	real-time motion detection (5 Mp color camera), ECG, breathing detection, temperature stabilization, all signals digitized in 16bit with up to 120 samples/sec
Radiation Safety	<1 µSv/h at any place of the instrument surface
System Dimensions	954W x 1190D x 940H mm, 360 kg

Fig. 3. Micro-CT Bruker 1276 Scanner specifications including size and technical data (Adelaide_Microscopy, 2022).

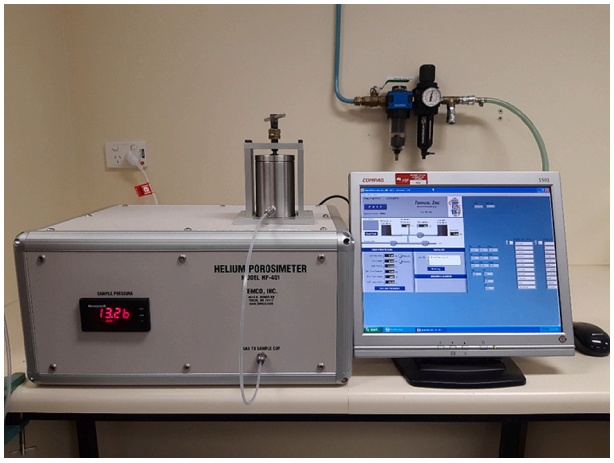

Fig. 4. The helium porosimeter used in this study is the HP-401 model manufactured by the TEMCO.

which is used for fracture analysis.

3. Experimental set up and methods

CO_2 and air flooding experiments, micro-CT scan imaging, and helium porosity measurements are performed to examine the changes in pore structure of the coal during CO_2 injection. The CO_2 flooding experiments are carried out using an in-house CO_2 flooding facility. A core plug, measuring 47 mm in length and 34 mm in diameter, is drilled parallel to the coal bedding from a core sample obtained from the study well (see Fig. 2).

3.1. Micro-CT scan imaging

Micro-CT scanning is conducted on the sample before and after performing CO_2 flooding experiments using the micro-CT Bruker 1276 Scanner, as depicted in Fig. 3. The scanning process involves capturing images of the sample at 360° with a rotation step of 0.2°, utilizing a resolution of 13 µm. These scanning parameters ensure high-resolution images of the sample, which are subsequently processed to generate 3D models of the pore structure, including natural fractures, cleats and master-cleats (large cleats that cut coal lithotype layers (Dawson and Esterle, 2010)). Additionally, the Bruker's Micro-CT Software CTAn is employed to create clear section cut images. The program CTvol is used for visualizing the 3D models. Refer to Fig. 3 for further details regarding the micro-CT scanner specifications.

3.2. Helium porosimeter

The helium porosimeter used in this study is the HP-401 model manufactured by TEMCO. It is designed to measure effective porosity of

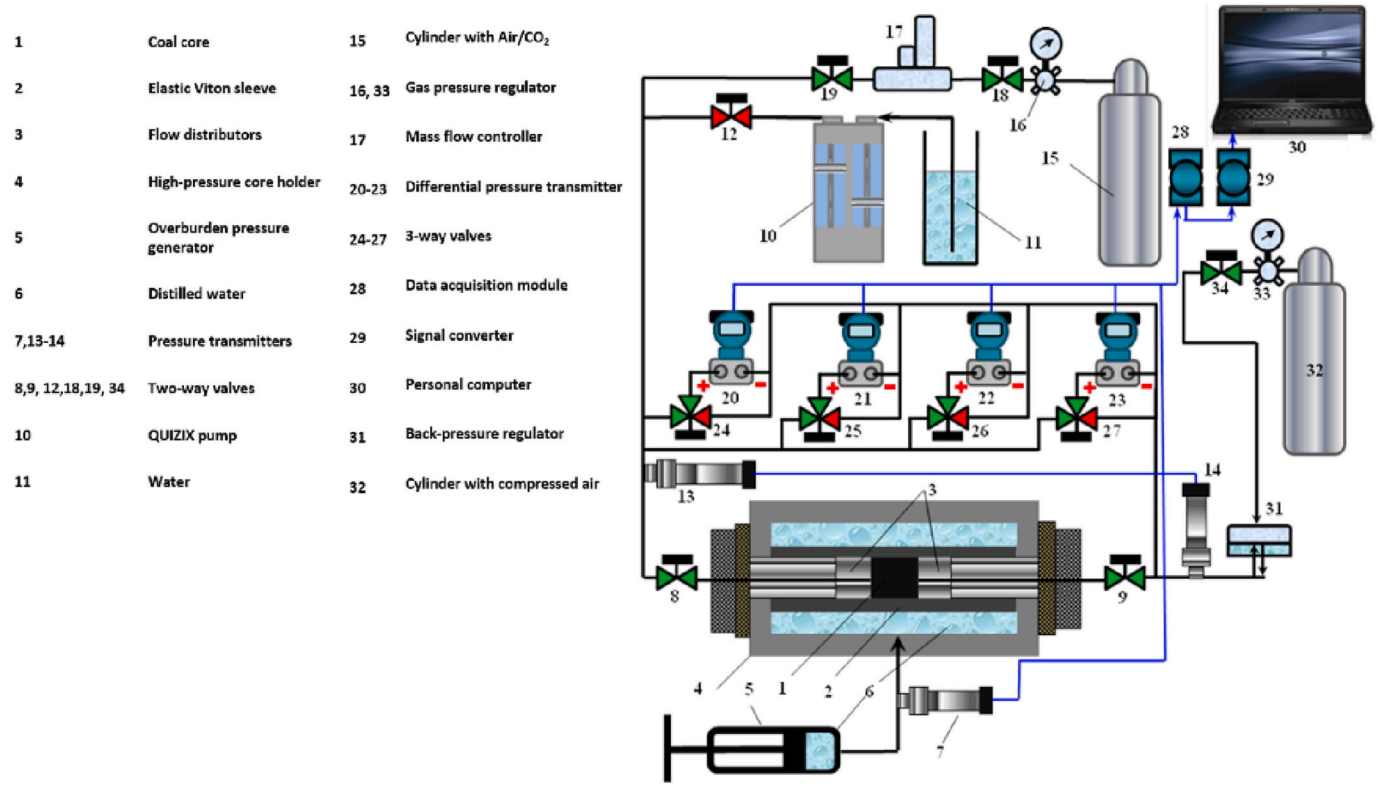

Fig. 5. The schematic of the Air/CO_2 core flooding facility used to measure coal permeability prior to, during, and after CO_2 flooding.

Table 1
Effective porosity of the coal sample measured by helium porosimeter before and after CO_2 flooding tests.

	Before CO_2 flooding	After CO_2 flooding
Trial 1	10.80%	6.14%
Trial 2	11.42%	6.37%
Trial 3	10.89%	6.38%
Average effective porosity	11.04%	6.29%

core samples. The porosimeter operates based on the Boyle's law and utilises helium gas due to its ideal gas behaviour and non-interaction with the coal. The measurement process involves three steps. Prior to each step, the gas chamber is evacuated using a vacuum pump to remove air. In the first step, the volume and pressure of the chamber are recorded when it is empty. This serves as a reference point for Boyle's law. The second step involves placing a cylindrical non-porous core made of lead in the chamber. The volume and pressure of helium are recorded to obtain the pressure when the porosity is zero. This helps to establish a baseline for comparison. In the third step, the coal sample is placed in the chamber, and the volume and pressure of helium are recorded. Using the data obtained from this step, the porosity of the coal sample is calculated. Fig. 4 shows the helium porosimeter used in this study to measure effective porosity.

3.3. CO_2 flooding experiment

CO_2 core flooding experiments are performed to measure coal permeability under various stresses during CO_2 flooding, while air core flooding experiments obtain coal permeability prior to and after CO_2 flooding experiments. This establishes a baseline for comparison of how the pore structure of the coal and resultant permeability alter during CO_2 tests. Fig. 5 shows the schematic of the CO_2 flooding experimental set up. The core plug (1) is tightly wrapped with Teflon tape to eliminate air and CO_2 leakage between the outer surface of the core and the Viton sleeve. The core plug, the Viton sleeve and two stainless-steel flow-distributors (3) are mounted inside the high-pressure core holder (4). Overburden pressure is created by a manual pressure generator (5) compressing distilled water (6) and measured by an absolute pressure transmitter (7) with a measuring pressure range of 0 to 30 MPa. Two-way manual valves (8) and (9) separated the core holder from the remaining system. Prior to testing on the coal sample, the system is tested by measuring liquid permeability of Berea core. A high-pressure pump (10) is used to perform core flooding with a high-salinity sodium chloride solution (11) (0.6 M NaCl). The obtained results in liquid permeability of the Berea core are within 3.2% with our previous results. The liquid injection system is separated from the gas injection system by a two-way shut-off valve (12). Absolute pressure transmitters (13) and (14) measure inlet and outlet pressures on the coal sample. A compressed gas cylinder (15) (Air and/or CO_2) delivers gaseous CO_2 to the core inlet via a pressure regulator (16), two-way mass flow controller (17), and two-way valves (18) and (19). Pressure drop across the core is measured by four differential pressure transmitters (20−23) with differential pressure ranges of 0 to 0.004 MPa, 0 to 0.1 MPa, 0 to 0.5 MPa, and 0 to 14 MPa. Pressure drops higher than 14 MPa can be measured by absolute pressure transmitters (13) and (14). These differential pressure transmitters are connected to the core-holder and the remaining tubing by three-way valves (24–27). Output signals from absolute pressure and differential pressure transmitters are fed into a data acquisition system comprising a signal conditioner (28), an analogue input module (29), and a desktop computer (30). Back-pressure regulator (31) is used to control the effective stress on the coal core. A compressed air cylinder (32) delivers air to the back-pressure regulator via a pressure regulator (33) and two-way valve (34). The effluent CO_2 stream from the core holder is delivered to a fume cabinet.

We adopted the following stages in the experimental procedure:

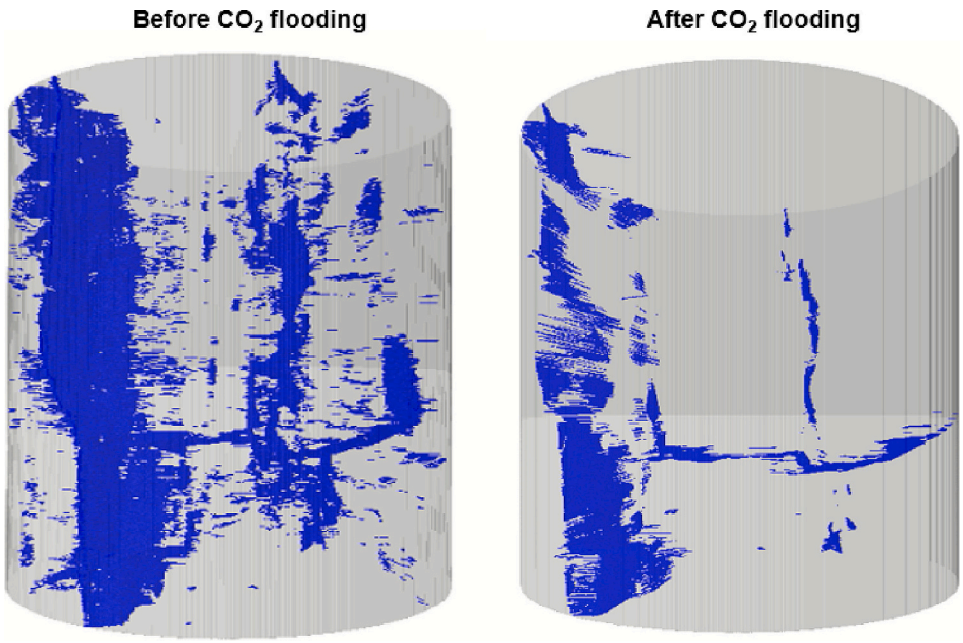

Fig. 6. The 3D models of the coal sample before and after CO_2 flooding experiments. The blue colour shows the pore structure including fractures, cleats, and master-cleats throughout the sample. The comparison reveals that CO_2 flooding resulted in significant irreversible changes to the pore structure of the coal. (For interpretation of the references to colour in this figure legend, the reader is referred to the web version of this article.)

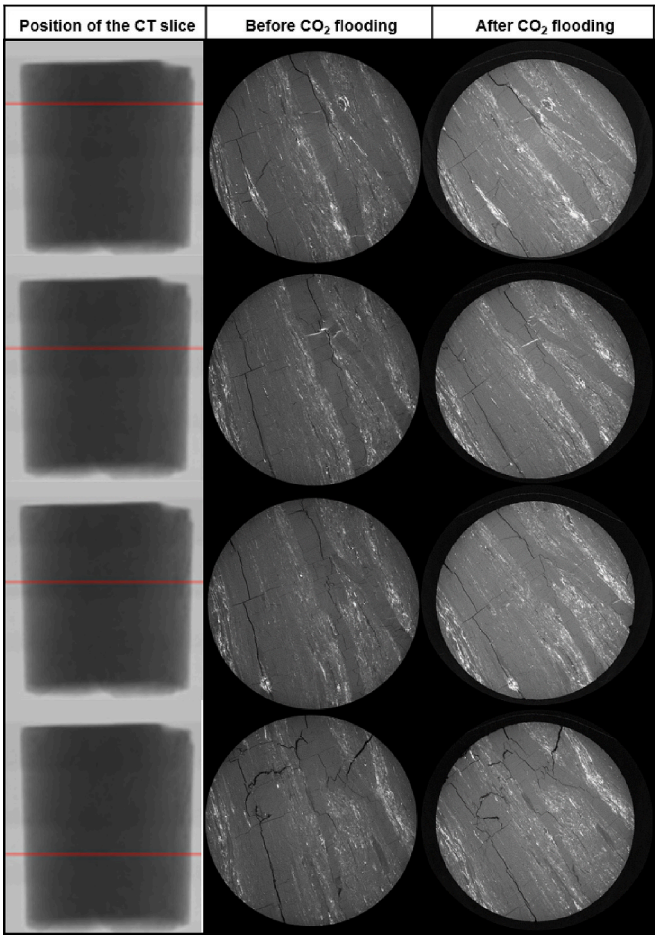

Fig. 7. CT scan images at different positions along the coal sample before and after CO_2 flooding experiments.

a. Permeability hysteresis removal is carried out to obtain consistent results from the planned tests on CO_2 injection into the coal core. During this procedure compressed air is injected at an average volumetric flowrate of 8.691×10^{-8} m^3/s or 50.936 sccm (standard cubic centimetres per minute), which is equivalent to 8.587×10^{-7} m^3/s at coal core conditions. The overburden pressure (P_{ob}) is maintained at 6.895 ± 0.010 MPa during all three stages of the experiment. Pore/fracture pressure (P_p) varies from 0.207 MPa to 6.136 MPa by varying compressed air pressure at the back-pressure regulator. Thus, after three cycles of increasing/decreasing of effective stresses, we have achieved the absence of hysteresis in the pressure drop across the coal core. Pressure drop across the core is measured in real-time mode and gas permeabilities are recorded. All experimental stages are carried out at room temperature controlled at 22.0 ± 0.5 °C.
b. Hysteresis removal is followed by injection of CO_2 at an average volumetric flowrate of 2.952×10^{-8} m^3/s or 50.617 sccm, which is equivalent to 8.436×10^{-7} m^3/s at coal core conditions. The pressure drop across the core is measured in real-time mode, and gas permeabilities are recorded.
c. Compressed air is injected into the coal core during the last stage of the gas core flooding procedure. Average air injection volumetric flowrate is 6.081×10^{-8} m^3/s or 50.588 sccm, which is equivalent to 8.431×10^{-7} m^3/s at coal core condition. The variation of P_p ranges from 0.401 MPa to 6.184 MPa by changing the compressed air pressure at the back-pressure regulator. During this procedure we determine whether there are irreversible changes in fracture/cleat network of the coal.
d. Upon completion of core flooding experiments, the core plug is removed from the core holder, and helium porosity tests and micro-CT scanning are performed on this core to investigate how CO_2 flooding impacted fracture/cleat network of the coal.

3.4. Borehole image log analysis

Borehole image logging is a technique to obtain a circumferential image of the borehole wall, providing valuable information for the interpretation of planar geological structures such as faults and fractures

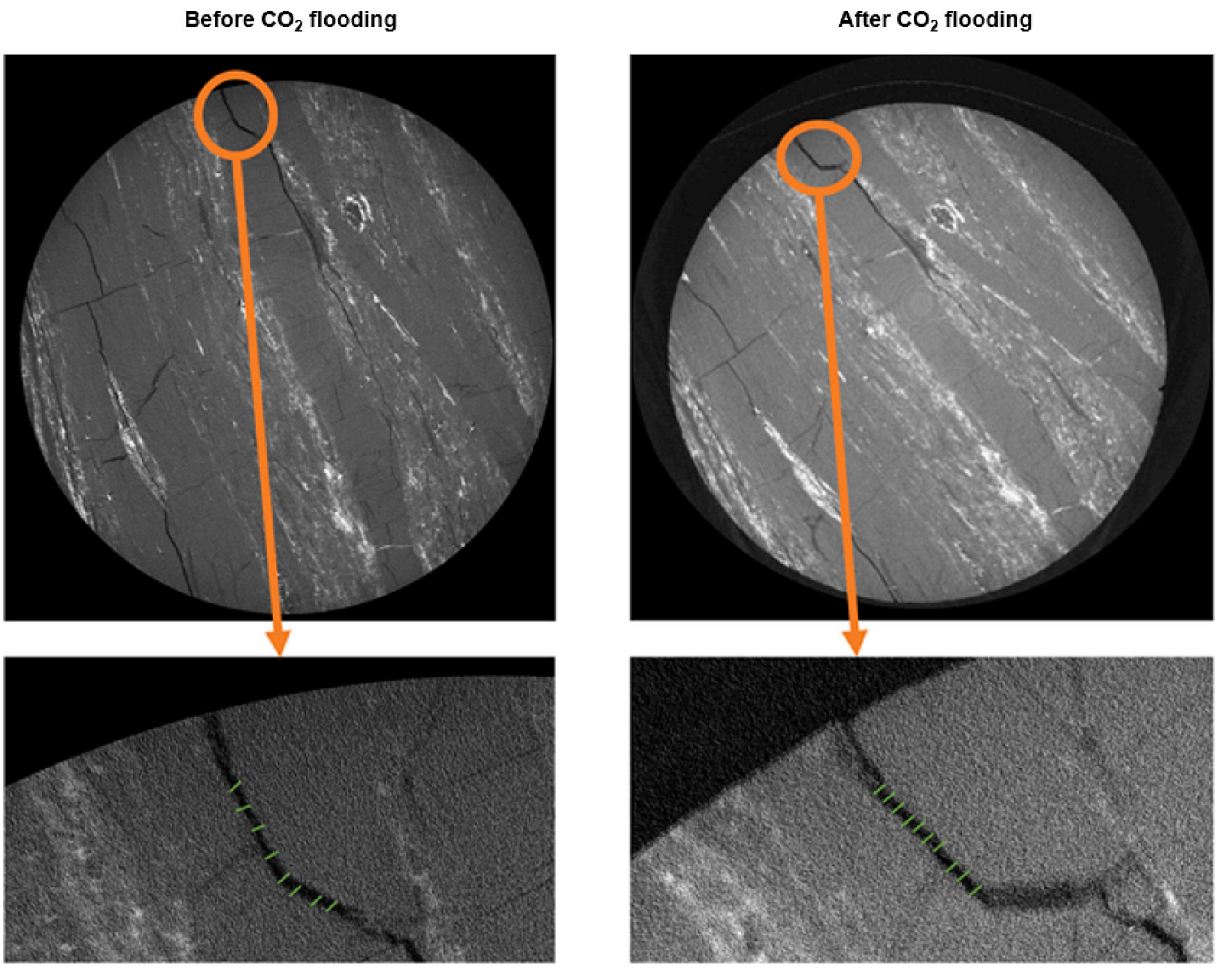

Fig. 8. Illustration of the mean aperture measurement of the fracture before and after CO_2 flooding experiments.

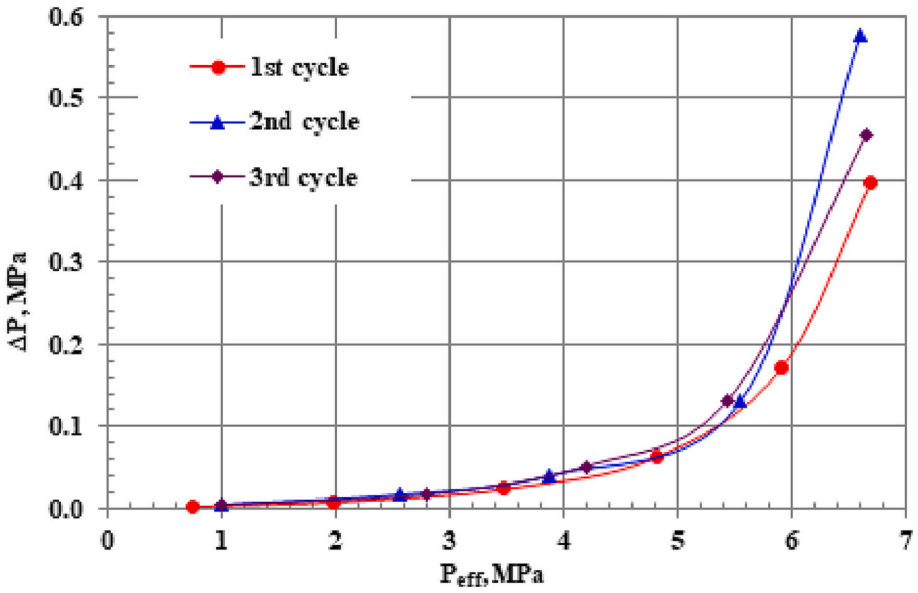

Fig. 9. Hysteresis removal during air core flooding experiments. Pressure drop results are consistent after three cycles for effective stresses lower than 5 MPa.

within formations. It also aids in the analysis of in-situ stresses and lithology identifications (Finkbeiner et al., 1997; Prensky, 1999; Rajabi et al., 2010; Rajabi et al., 2016, Ranjbar-Karami et al., 2019). In this study, we analyzed the acoustic borehole image log of the study wellbore to characterize the fracture pattern within coal seams by examining travel time and amplitude of reflected signals recorded during logging (Mukherjee et al., 2021; Prensky, 1999; Rajabi et al., 2022).

Cross-formational flow, which is an environmental concern

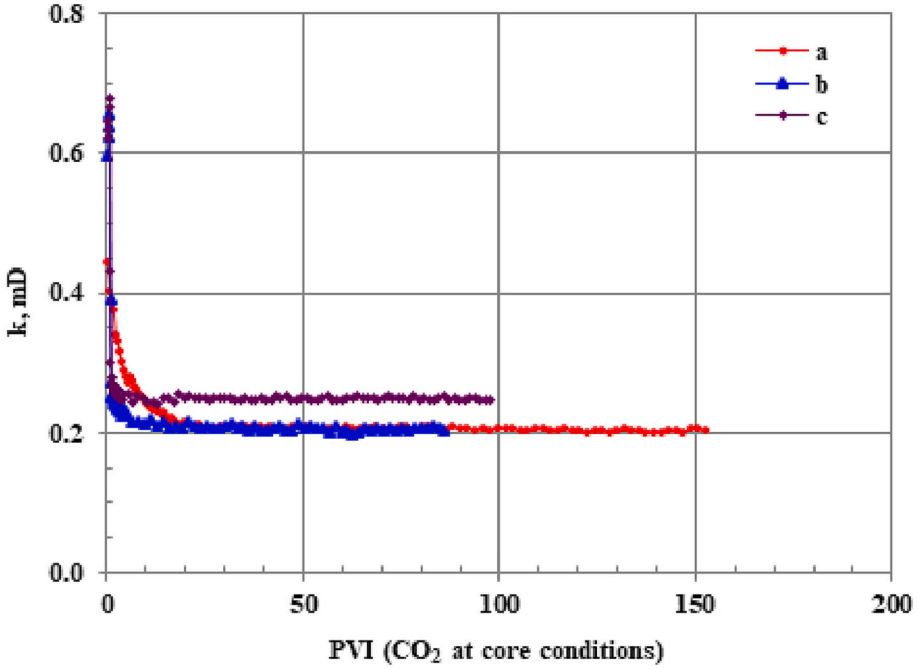

Fig. 10. Permeability versus pore volume injected (at core conditions), (a) effective stress is 3.955 ± 0.029 MPa (573.6 ± 4.3 psi), (b) effective stress is 3.220 ± 0.016 MPa (467.1 ± 2.3 psi), and (c) effective stress is 2.472 ± 0.011 MPa (358.6 ± 0.4 psi).

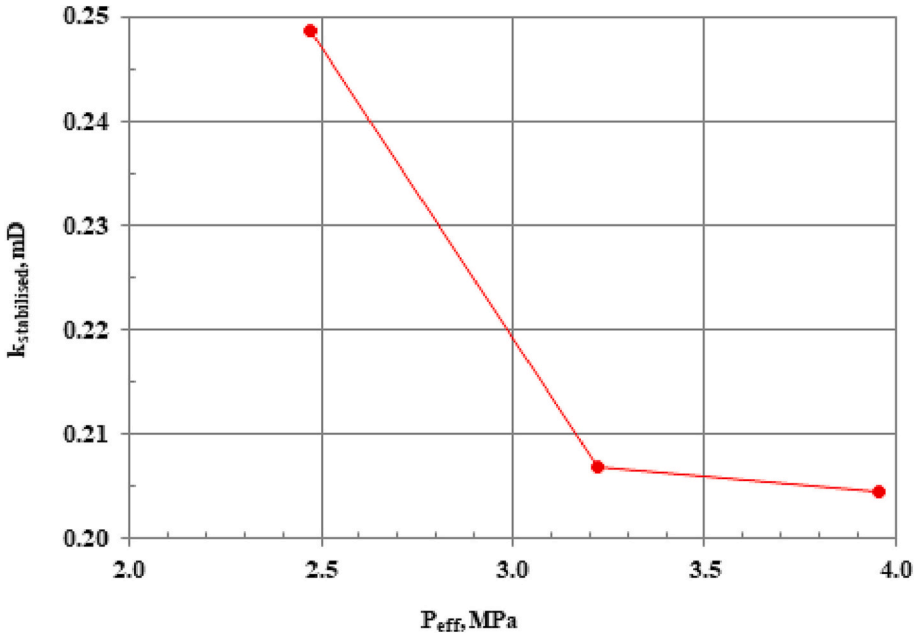

Fig. 11. Coal permeability versus effective stress during CO_2 core flooding experiments.

associated with coal seam gas activities, including CO_2 sequestration, can occur due to various factors. These factors can be intrinsic, related to geological setting of the area, or extrinsic, for example related to well completion practices. Intrinsic factors, such as tectonic stresses and geological structures like faults and fractures, can increase the likelihood of hydraulic communication (Salmachi and Karacan, 2017). Faults can juxtapose aquifers to coal seams or serve as a pathway for fluid transmission when they are suitably oriented in relation to the in-situ stresses. Fractures can also facilitate fluid exchange between different geological formations if they are (sub-) parallel to the direction of maximum horizontal stress (Rajabi et al., 2016). Hydraulic conductivity of faults and fractures depends on their characteristics relative to the present-day tectonic stress regime (Mukherjee et al., 2021; Mukherjee et al., 2020; Salmachi and Karacan, 2017). Hence, analyzing the fracture system within coal seams using the borehole image log provides valuable information including fracture intensity, openness, and their extension to non-coal neighbouring formations. This information is crucial for assessing the potential of cross-formational flow during CO_2 sequestration. It should be noted that results from borehole image log analysis must be considered in conjunction with other analysis and information for a comprehensive assessment of likelihood of cross-formational flow.

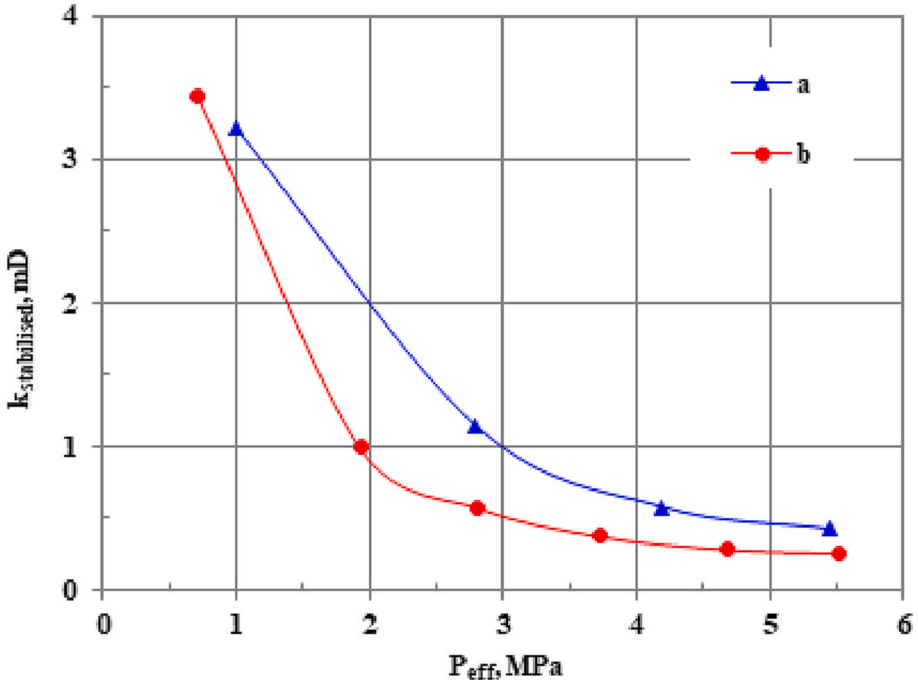

Fig. 12. Permeability versus effective stress (a) before and (b) after CO_2 core flooding experiments. Note that in this figure permeability values are measured using air. Permeability values, measured after CO_2 flooding experiments, are consistently lower than those measured prior to CO_2 flooding tests. This demonstrates the irreversible changes to the pore structure of the coal.

4. Results and discussions

The pore structure of the coal undergoes irreversible changes after CO_2 flooding tests are completed and CO_2 is removed from the coal matrix. While changes in pore sizes induced by CO_2 adsorption is reversible upon desorption of CO_2, significant irreversible alterations in the pore structure are observed in this study. This suggests the occurrence of permeant damage that cannot be restored. A comparison of experimental results obtained before and after CO_2 flooding experiments clearly demonstrates the irreversible changes in the pore structure.

The results of the helium porosimeter tests conducted prior to and after the CO_2 flooding experiments are presented in Table 1. Three trials were conducted and an average value for effective porosity was calculated. The results indicate a decrease in effective porosity by approximately 43% after CO_2 injection.

The decline in effective porosity, as measured by helium porosimeter, is consistent with findings of micro-CT scan imaging of the coal sample. The impact of CO_2 on the pore structure of the sample is clearly evident in the constructed 3D models using the CT slices (see Fig. 6). The pore structure of the sample, including fractures, cleats, and master-cleats, is presented by the blue colour. The reduction in size and closure of fractures and cleats after CO_2 flooding tests are visible. Fig. 7 shows different CT slices along the coal sample prior to and after CO_2 flooding experiments, along with their corresponding positions along the sample. The two main fractures/cleats are observed consistently throughout the sample with numerous connected and isolated cleats. Some cleats have undergone complete or partial closure, while the main two fractures/cleats throughout the sample remain open despite a reduction in aperture size (see Fig. 6 and Fig. 7).

The mean aperture of one of the main fractures/cleats was measured prior to and after CO_2 flooding experiments by taking 10 measurement points along the fracture/cleat (see Fig. 8). The results show a reduction in mean aperture from 124.25 μm to 95.15 μm, representing a decrease of approximately 23%. Liu et al. (2022) reported original mean aperture sizes of 27.24 μm, 29.46 μm, and 19.21 μm in three flow directions reduced by 80%, 79%, and 88%, respectively after injecting CO_2 with an injection pressure of 3 MPa. It is important to note that their measurements were taken during CO_2 flooding experiments, encompassing both reversible and irreversible changes. In our study, measurements are taken after CO_2 flooding experiments, specifically capturing the irreversible changes in the pore structure. The difference in measurement timing accounts for the contrasting results between the two studies.

Fig. 9 shows the results of hysteresis removal associated with permeability measurements by air core flooding. This ensures all CO_2 flooding experiments are performed within the 'NO-hysteresis' range as indicated in Fig. 9. The effective stresses used in experiments are 3.955 $\pm$ 0.029 MPa, 3.220 $\pm$ 0.016 MPa, and 2.472 $\pm$ 0.011 MPa.

At the beginning of each CO_2 flooding test, permeability rapidly declines and then reaches a stable state (see Fig. 10). The first CO_2 flooding test is conducted at an effective stress of 3.955 MPa. Once pressure drop across the core stabilizes for 24 h, permeability is measured. Subsequently, the pore pressure is increased while the overburden pressure is kept constant, resulting in reduction of effective stress toward the next measurement point. This procedure is repeated to measure permeability at other points. The pressure drop across the core stabilizes after a certain volume of CO_2, expressed as PVI (pore volume injected), has been injected. Specifically, the pressure drop stabilizes after 31.6 PVI, 12.7 PVI, and 5.31 PVI for the aforementioned effective stresses, respectively. This stabilization indicates that the coal sample has been saturated with CO_2 at that particular pore pressure, and no further adsorption or reduction occurs at that stage.

The decline in permeability at a given effective stress is attributed to coal matrix swelling, narrowing down fracture/cleat apertures throughout the coal. At lower pore pressures (higher effective stresses), there are plenty of adsorption sites in coal to receive CO_2, resulting in higher PVI before saturation is reached and permeability stabilizes. When the effective stress decreases from 3.955 MPa to 3.220 MPa in the second test, change in permeability is negligible. This indicates that the effect of pore compressibility offsets the effect of matrix swelling at higher pore pressures (lower effective stresses). In the third test, at an effective stress of 2.472 MPa, permeability increases by 20% compared to the second test, owing to the dominance of pore compressibility effect

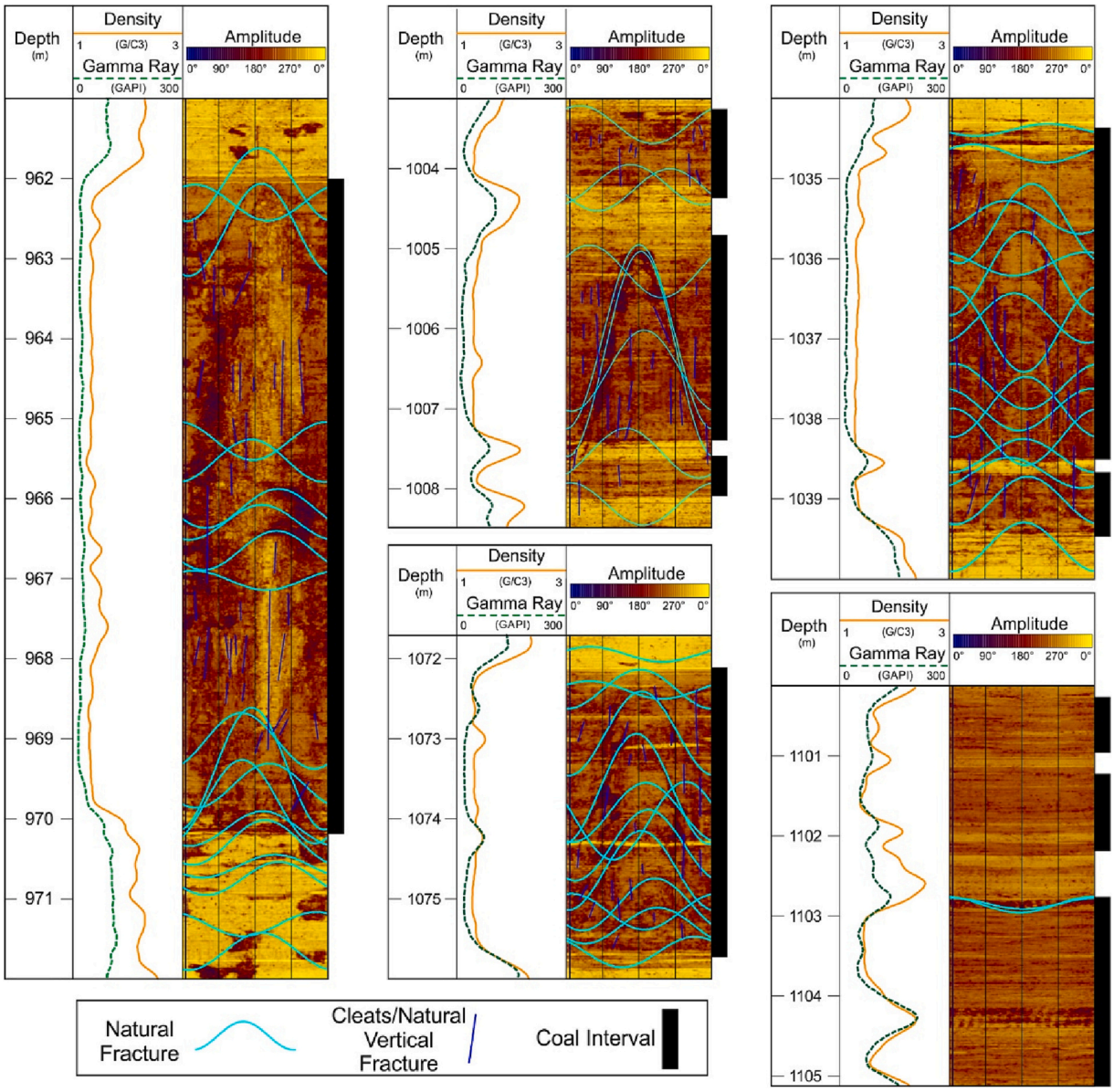

Fig. 13. Borehole image logs for coal seams intersected in the study well. Borehole image logs show the natural fracture/cleat intensity in each coal seam. The majority of natural fractures are confined within coal seams, with only a few fractures propagate into the non-coal adjacent strata.

over the matrix swelling. The results for permeability measurements at the three different effective stresses are shown in Fig. 11.

The interaction between the coal matrix and CO_2 leads to changes in the pore structure, resulting in a decrease in permeability during CO_2 injection at a given effective stress. This phenomenon has been documented by various authors in the literature, including Liu and Rutqvist (2010), Liu et al. (2017) and Peng et al. (2014). Permeability measurements conducted at different effective stresses indicate that the combined effects of matrix swelling and pore compressibility, two opposing factors, determine the changes in permeability. These findings are consistent with previous studies conducted by Fujioka et al. (2010), Gruszkiewicz et al. (2009), Harpalani and Chen (1995), Liu et al. (2022), Majewska et al. (2009) and Pan et al. (2010). The increase in permeability can be advantageous for maintaining injectivity during CO_2 sequestration projects.

Fig. 12 shows permeability at different effective stresses prior to and after CO_2 flooding experiments, as measured by compressed air. The air permeability measurements conducted after CO_2 core flooding experiments consistently exhibit lower values compared to the measurements prior to the tests. For instance, at an effective stress of 2.81 MPa, the permeability is reduced by approximately 50%, from 1.13 mD to 0.57 mD. During the CO_2 flooding test at this effective stress, measured permeability is 0.23 mD, which is lower than air flooding permeability. This comparison reveals that a portion of permeability loss is reversible and can be restored when CO_2 is desorbed from the coal matrix. However, some changes are irreversible, and the permeability does not return to its original values measured prior to the CO_2 flooding experiments. This observation is further supported by the results obtained from micro-CT scan images and helium porosimeter, which reveal significant changes in the pore structure of the coal, indicating the presence of permanent damage caused by CO_2 flooding.

The most likely mechanism responsible for permanent damage to coal permeability is chemisorption. The interaction between CO_2 and coal matrix results in formation of new compounds. This process, inherently irreversible, causes changes in physical and chemical structure of the coal, resulting in alteration to cleats and natural fractures, ultimately leading to a reduction in permeability.

Fig. 13 shows the interpreted natural fractures/cleats using borehole

image log analysis in the main coal seams (C2 and C3) of the study wellbore. The coal interval C2 spans from a depth of 963 m to 970 m, while C3 ranges from 1035 m to1039m. Natural fractures/cleats can be observed in both coal intervals, while C3 exhibits a higher fracture intensity compared to C2. The majority of fractures are confined within the coal intervals and do not extend into adjacent non-coal strata. Only a few fractures are observed to propagate into non-coal strata, both above and below the coal intervals. The lithology of strata in the vicinity of C2 and C3 predominantly consists of siltstone to very fine sandstone, with no visible fractures. This suggests that the hydraulic communication between the coal seams and neighbouring strata in this particular wellbore is relatively limited.

The results of this work provide valuable insights for CO_2 injection in depleted coal seam gas reservoirs by quantifying the magnitude of permanent damage to coal permeability and assessing combined effect of matrix shrinkage and pore compressibility on injectivity. Additionally, it introduces the novel application of borehole image logs in identifying cleats and natural fractures that can potentially facilitate hydraulic communication between storage site and adjacent strata.

5. Conclusions

This study aims to investigate the changes in the pore structure of the coal during the flow of CO2 in the gaseous form. Micro-CT scan imaging, CO_2 and air flooding experiments, and porosity measurements are conducted on a coal sample from the Bowen Basin. The research findings indicate that the pore structure of the coal undergoes both reversible and irreversible changes. After CO_2 flooding, the effective porosity of the coal sample is reduced by 43%. Additionally, the construction of 3D models of the pore structure using micro-CT scan images, reveals significant shrinkage in fracture aperture and complete or partial closure of cleats.

While a portion of permeability loss is reversible when CO_2 is desorbed from the coal matrix, permanent damage to the pore structure of the coal is irreversible. This is inferred by comparing coal permeability measurements using air prior to and after flooding experiments, as well as through analysis of the 3D models of the pore structure of the coal constructed prior to and after the CO_2 flooding tests. Irreversible changes have caused a 50% reduction in coal permeability. Although some micro-cleats are closed due to the permanent damage to the pore structure, the two major fractures/cleats throughout the core remain open despite a reduction in their sizes.

At lower effective stresses, the pore compressibility of the coal plays an important role in counteracting the swelling effect, leading to an improvement in permeability. This is crucial for maintaining injectivity during CO_2 sequestration.

Authorship statement

All persons who meet authorship criteria are listed as authors, and all authors certify that they have participated sufficiently in the work to take public responsibility for the content, including participation in the concept, design, analysis, writing, or revision of the manuscript. Furthermore, each author certifies that this material or similar material has not been and will not be submitted to or published in any other publication before its appearance in the International Journal of Coal Geology.

CRediT authorship contribution statement

Alireza Salmachi: Conceptualization, Supervision, Methodology, Validation, Formal analysis, Investigation, Resources, Data curation, Writing – original draft, Writing – review & editing, Visualization, Funding acquisition. **Abbas Zeinijahromi:** Conceptualization, Supervision, Validation, Investigation, Resources, Data curation, Writing – review & editing, Funding acquisition. **Mohammed Said Algarni:** Conceptualization, Methodology, Formal analysis, Writing – original draft. **Nawaf Abdullah Abahussain:** Conceptualization, Methodology, Formal analysis, Writing – original draft. **Saad Abdullah Alqahtani:** Conceptualization, Methodology, Formal analysis, Writing – original draft. **Alexander Badalyan:** Conceptualization, Supervision, Methodology, Formal analysis, Writing – review & editing, Validation, Investigation, Resources, Data curation. **Mohammad Rezaee:** Conceptualization, Methodology, Writing – original draft, Writing – review & editing. **Mojtaba Rajabi:** Conceptualization, Supervision, Methodology, Validation, Formal analysis, Investigation, Resources, Data curation, Writing – original draft, Writing – review & editing, Visualization, Funding acquisition.

Declaration of Competing Interest

The authors declare that they have no known competing financial interests or personal relationships that could have appeared to influence the work reported in this paper.

Data availability

The authors do not have permission to share data.

Acknowledgements

Contributions by Mojtaba Rajabi was supported through ARC Discovery Early Career Researcher Award (DE200101361).

References

Adelaide_Microscopy, 2022. X-ray Micro-Tomography (Micro-CT). Retrieved 1 June 2022, from. https://www.adelaide.edu.au/microscopy/facilities-services/instrumentation/x-ray-micro-tomography-micro-ct#information-on-the-micro-ct-bruker-1276-scanner.

Ahamed, M.A.A., Perera, M.S.A., Matthai, S.K., Ranjith, P.G., Dong-yin, L., 2019. Coal composition and structural variation with rank and its influence on the coal-moisture interactions under coal seam temperature conditions – a review article. J. Pet. Sci. Eng. 180, 901–917.

Ali, M., Jha, N.K., Pal, N., Keshavarz, A., Hoteit, H., Sarmadivaleh, M., 2022. Recent advances in carbon dioxide geological storage, experimental procedures, influencing parameters, and future outlook. Earth Sci. Rev. 225, 103895.

Bai, G., Su, J., Zhang, Z., Lan, A., Zhou, X., Gao, F., Zhou, J., 2022. Effect of CO2 injection on CH4 desorption rate in poor permeability coal seams: an experimental study. Energy 238, 121674.

Baker, J.C., Fielding, C.R., de Caritat, P., Wilkinson, M.M., 1993. Permian evolution of sandstone composition in a complex back-arc extensional to foreland basin; the Bowen Basin, eastern Australia. J. Sediment. Res. 63, 881–893.

Chen, Z., Liu, J., Pan, Z., Connell, L.D., Elsworth, D., 2012. Influence of the effective stress coefficient and sorption-induced strain on the evolution of coal permeability: Model development and analysis. Int. J. Greenh. Gas Cont. 8, 101–110.

Clarkson, C.R., Bustin, R.M., 2000. Binary gas adsorption/desorption isotherms: effect of moisture and coal composition upon carbon dioxide selectivity over methane. Int. J. Coal Geol. 42, 241–271.

Clarkson, C.R., Salmachi, A., 2017. Rate-transient analysis of an undersaturated CBM reservoir in Australia: Accounting for effective permeability changes above and below desorption pressure. J. Nat. Gas Sci. Eng. 40, 51–60.

Dawson, G.K.W., Esterle, J.S., 2010. Controls on coal cleat spacing. Int. J. Coal Geol. 82, 213–218.

Day, S., Fry, R., Sakurovs, R., 2008. Swelling of Australian coals in supercritical CO2. Int. J. Coal Geol. 74, 41–52.

Dong, H., Zhang, Y., Lebedev, M., Arif, M., Yuan, Y., Iglauer, S., 2021. Simulating coal permeability change as a function of effective stress using a microscale digital rock model. Energy Fuel 35, 8756–8762.

Draper, J.J., Boreham, C.J., 2006. Geological controls on exploitable coal seam gas distribution in Queensland. APPEA J. 46, 343–366.

Du, X., Cheng, Y., Liu, Z., Yin, H., Wu, T., Huo, L., Shu, C., 2021. CO2 and CH4 adsorption on different rank coals: a thermodynamics study of surface potential, Gibbs free energy change and entropy loss. Fuel 283, 118886.

Esen, O., Özer, S.C., Soylu, A., Ramazani Rend, A., Fişne, A., 2020. Geological controls on gas content distribution of coal seams in the Kınık coalfield, Soma Basin, Turkey. Int. J. Coal Geol. 231, 103602.

Fan, C., Yang, L., Sun, H., Luo, M., Zhou, L., Yang, Z., Li, S., 2023. Recent advances and Perspectives of CO2-Enhanced Coalbed methane: Experimental, Modeling, and Technological Development. Energy Fuel 37, 3371–3412.

Ferguson, R.M., 2008. Climate Change 2007: Mitigation of climate Change - Contribution of Working Group III to the Fourth Assessment Report of the Intergovernmental

Panel on Climate Change. (Book review). CHOICE: Current Reviews for Academic Libraries, 45. American Library Association, Middletown, p. 1570.
Finkbeiner, T., Barton, C.A., Zoback, M.D., 1997. Relationships among in-situ stress, fractures and faults, and fluid flow: Monterey formation, Santa Maria Basin, California. Am. Assoc. Pet. Geol. Bull. 81, 1975–1999.
FrOG-Tech, 2006. OZ SEEBASE Proterozoic Basins Study, Report to Geoscience Australia by FrOG. Tech Pty Ltd.
Fujioka, M., Yamaguchi, S., Nako, M., 2010. CO2-ECBM field tests in the Ishikari Coal Basin of Japan. Int. J. Coal Geol. 82, 287–298.
Gao, Z., Li, B., Li, J., Wang, B., Ren, C., Xu, J., Chen, S., 2021. Coal permeability related to matrix-fracture interaction at different temperatures and stresses. J. Pet. Sci. Eng. 200, 108428.
Green, P., Hoffmann, K., Brain, T., Gray, A., 1997. The Surat and Bowen Basins, South-East Queensland. Queensland Department of Mines and Energy.
Gruszkiewicz, M.S., Naney, M.T., Blencoe, J.G., Cole, D.R., Pashin, J.C., Carroll, R.E., 2009. Adsorption kinetics of CO2, CH4, and their equimolar mixture on coal from the Black Warrior Basin, West-Central Alabama. Int. J. Coal Geol. 77, 23–33.
Hadi Mosleh, M., Sedighi, M., Babaei, M., Turner, M., 2019. 16 - Geological sequestration of carbon dioxide. In: Letcher, T.M. (Ed.), Managing Global Warming. Academic Press, pp. 487–500.
Han, J., Wu, C., Jiang, X., Fang, X., Zhang, S., 2022. Investigation on effective stress coefficients and stress sensitivity of different water-saturated coals using the response surface method. Fuel 316, 123238.
Harpalani, S., Chen, G., 1995. Estimation of changes in fracture porosity of coal with gas emission. Fuel 74, 1491–1498.
Hong, W.Y., 2022. A techno-economic review on carbon capture, utilisation and storage systems for achieving a net-zero CO2 emissions future. Carbon Capture Sci. Technol. 3, 100044.
Jell, P., 2013. Geology of Queensland. Geological Survey of Queensland, Brisbane, Queensland.
Jia, Q., Liu, D., Cai, Y., Fang, X., Li, L., 2020. Petrophysics characteristics of coalbed methane reservoir: a comprehensive review. Front. Earth Sci. 1–22.
Jinlong, J., Liwen, C., 2020. An experimental study on the permeability changes of anthracite reservoirs in different depths of Qinshui Basin induced by supercritical CO2 injection. Energy Sci. Eng. 8, 849–864.
Korsch, R.J., Totterdell, J.M., 2009a. Evolution of the Bowen, Gunnedah and Surat Basins, eastern Australia. Aust. J. Earth Sci. 56, 271–272.
Korsch, R.J., Totterdell, J.M., 2009b. Subsidence history and basin phases of the Bowen, Gunnedah and Surat Basins, eastern Australia. Aust. J. Earth Sci. 56, 335–353.
Korsch, R., Totterdell, J., Cathro, D., Nicoll, M., 2009. Early Permian east Australian rift system. Aust. J. Earth Sci. 56, 381–400.
Krooss, B.M., van Bergen, F., Gensterblum, Y., Siemons, N., Pagnier, H.J.M., David, P., 2002. High-pressure methane and carbon dioxide adsorption on dry and moisture-equilibrated Pennsylvanian coals. Int. J. Coal Geol. 51, 69–92.
Larsen, J.W., Green, T.K., Kovac, J., 1985. The nature of the macromolecular network structure of bituminous coals. J. Org. Chem. 50, 4729–4735.
Li, D., Liu, Q., Weniger, P., Gensterblum, Y., Busch, A., Krooss, B.M., 2010. High-pressure sorption isotherms and sorption kinetics of CH4 and CO2 on coals. Fuel 89, 569–580.
Li, J., Li, B., Cheng, Q., Gao, Z., 2022. Characterization of anisotropic coal permeability with the effect of sorption-induced deformation and stress. Fuel 309, 122089.
Li, J., Pan, J., Wang, X., Wang, K., Nie, S., Gao, D., 2023. Potential effect of carbon dioxide injection on the functional groups of medium volatile bituminous coals analysed using in-situ diffuse reflectance Fourier-transform infrared spectroscopy. Int. J. Coal Geol. 265, 104169.
Lin, Y., Qin, Y., Ma, D., Zhao, J., 2020. Experimental Research on Dynamic Variation of Permeability and Porosity of Low-Rank Inert-Rich Coal under Stresses. ACS Omega 5, 28124–28135.
Liu, H.-H., Rutqvist, J., 2010. A New Coal-Permeability Model: Internal Swelling Stress and Fracture–Matrix Interaction. Transp. Porous Media 82, 157–171.
Liu, T., Lin, B., Yang, W., 2017. Impact of matrix–fracture interactions on coal permeability: model development and analysis. Fuel 207, 522–532.
Liu, C., Sang, S., Fan, X., Zhang, K., Song, F., Cui, X., Wang, H., 2020. Influences of pressures and temperatures on pore structures of different rank coals during CO2 geological storage process. Fuel 259, 116273.
Liu, Y., Lebedev, M., Zhang, Y., Wang, E., Li, W., Liang, J., Feng, R., Ma, R., 2022. Micro-Cleat and Permeability Evolution of Anisotropic Coal during Directional CO2 Flooding: an in Situ Micro-CT Study. Nat. Resour. Res. 31, 2805–2818.
Majewska, Z., Ceglarska-Stefańska, G., Majewski, S., Ziętek, J., 2009. Binary gas sorption/desorption experiments on a bituminous coal: Simultaneous measurements on sorption kinetics, volumetric strain and acoustic emission. Int. J. Coal Geol. 77, 90–102.
Martin-Roberts, E., Scott, V., Flude, S., Johnson, G., Haszeldine, R.S., Gilfillan, S., 2021. Carbon capture and storage at the end of a lost decade. One Earth 4, 1569–1584.
Mathews, J.P., Campbell, Q.P., Xu, H., Halleck, P., 2017. A review of the application of X-ray computed tomography to the study of coal. Fuel 209, 10–24.
Mazumder, S., Wolf, K.H., 2008. Differential swelling and permeability change of coal in response to CO2 injection for ECBM. Int. J. Coal Geol. 74, 123–138.
Moffat, D.H., Weale, K.E., 1955. Sorption by coal of methane at high pressures. Fuel 34, 449–462.
Mukherjee, M., Misra, S., 2018. A review of experimental research on Enhanced Coal Bed methane (ECBM) recovery via CO2 sequestration. Earth Sci. Rev. 179, 392–410.
Mukherjee, S., Rajabi, M., Esterle, J., Copley, J., 2020. Subsurface fractures, in-situ stress and permeability variations in the Walloon Coal measures, eastern Surat Basin, Queensland, Australia. Int. J. Coal Geol. 222, 103449.
Mukherjee, S., Rajabi, M., Esterle, J., 2021. Relationship between coal composition, fracture abundance and initial reservoir permeability: a case study in the Walloon Coal measures, Surat Basin, Australia. Int. J. Coal Geol. 240, 103726.
Niu, Q., Cao, L., Sang, S., Zhou, X., Liu, S., 2019. Experimental study of permeability changes and its influencing factors with CO2 injection in coal. J. Nat. Gas Sci. Eng. 61, 215–225.
Pan, Z., Connell, L.D., Camilleri, M., 2010. Laboratory characterisation of coal reservoir permeability for primary and enhanced coalbed methane recovery. Int. J. Coal Geol. 82, 252–261.
Peng, Y., Liu, J., Wei, M., Pan, Z., Connell, L.D., 2014. Why coal permeability changes under free swellings: New insights. Int. J. Coal Geol. 133, 35–46.
Prensky, S.E., 1999. Advances in borehole imaging technology and applications. Geol. Soc. Lond., Spec. Publ. 159, 1–43.
Qi, L., Tang, X., Wang, Z., Peng, X., 2017. Pore characterization of different types of coal from coal and gas outburst disaster sites using low temperature nitrogen adsorption approach. Int. J. Min. Sci. Technol. 27, 371–377.
Rajabi, M., Sherkati, S., Bohloli, B., Tingay, M., 2010. Subsurface fracture analysis and determination of in-situ stress direction using FMI logs: an example from the Santonian carbonates (Ilam Formation) in the Abadan Plain, Iran. Tectonophysics 492, 192–200.
Rajabi, M., Tingay, M., Heidbach, O., 2016. The present-day state of tectonic stress in the Darling Basin, Australia: Implications for exploration and production. Mar. Pet. Geol. 77, 776–790.
Rajabi, M., Esterle, J., Heidbach, O., Travassos, D., Fumo, S., 2022. Characterising the contemporary stress orientations near an active continental rifting zone: a case study from the Moatize Basin, Central Mozambique. Basin Res. 34, 1292–1313.
Ranathunga, A.S., Perera, M.S.A., Ranjith, P.G., Rathnaweera, T.D., Zhang, X.G., 2017. Effect of coal rank on CO2 adsorption induced coal matrix swelling with different CO2 properties and reservoir depths. Energy Fuel 31, 5297–5305.
Ranjbar-Karami, R., Rajabi, M., Ghavidel, A., Afroogh, A., 2019. Contemporary tectonic stress pattern of the Persian Gulf Basin, Iran. Tectonophysics 766, 219–231.
Rogers, R.E., Ramurthy, K., Rodvelt, G., Mullen, M., Company, H., 2007. Coalbed Methane: Principles and Practices, Oktibbeha. Oktibbeha.
Salmachi, A., Haghighi, M., 2012. Temperature effect on methane sorption and diffusion in coal: application for thermal recovery from coal seam gas reservoirs. APPEA J. 52, 291–300.
Salmachi, A., Karacan, C.Ö., 2017. Cross-formational flow of water into coalbed methane reservoirs: controls on relative permeability curve shape and production profile. Environ. Earth Sci. 76, 200.
Salmachi, A., Rajabi, M., Wainman, C., Mackie, S., McCabe, P., Camac, B., Clarkson, C., 2021. History, Geology, in Situ stress Pattern, Gas Content and Permeability of Coal Seam Gas Basins in Australia: a Review. Energies 14, 2651.
Shaw, R., Mukherjee, S., 2022. The development of carbon capture and storage (CCS) in India: a critical review. Carbon Capture Sci. Technol. 100036.
Su, E., Liang, Y., Zou, Q., Niu, F., Li, L., 2019. Analysis of effects of CO2 injection on coalbed permeability: implications for coal seam CO2 sequestration. Energy Fuel 33, 6606–6615.
Totterdell, J.M., Moloney, J., Korsch, R.J., Krassay, A.A., 2009. Sequence stratigraphy of the Bowen–Gunnedah and Surat Basins in New South Wales. Aust. J. Earth Sci. 56, 433–459.
Wang, G., Jiang, C., Shen, J., Han, D., Qin, X., 2019. Deformation and water transport behaviors study of heterogenous coal using CT-based 3D simulation. Int. J. Coal Geol. 211, 103204.
Wang, B., Wu, Y., Li, G., Yang, J., Zhao, Y., Wang, M., Zhou, J., Wu, T., Pan, Z., 2022. Laboratory study of fracture permeability of mineral-filled coal from Fanzhuang Block, southern Qinshui Basin, China. J. Pet. Sci. Eng. 208, 109799.
Wong, K.F., 2015. Climate Change. Momentum Press.
Xin, T., Liang, B., Wang, J., Sun, W., Sun, Y., 2021. Experimental Study on the Evolution Trend of the Pore Structure and the Permeability of coal under Cyclic Loading and unloading. ACS Omega 6, 35830–35843.
Yarmohammadtooski, Z., Salmachi, A., White, A., Rajabi, M., 2017. Fluid flow characteristics of Bandanna Coal Formation: a case study from the Fairview Field, eastern Australia. Aust. J. Earth Sci. 64, 319–333.
Yuan, T., Wei, Y., Chen, S., Liu, W., Zhao, L., Zhang, X., 2022. Study on Mechanical Properties and Crack Propagation of Raw Coal with Different Bedding Angles based on CT Scanning. ACS Omega 7, 27185–27195.
Zhang, Y., Lebedev, M., Sarmadivaleh, M., Barifcani, A., Rahman, T., Iglauer, S., 2016. Swelling effect on coal micro structure and associated permeability reduction. Fuel 182, 568–576.
Zhang, L., Kan, Z., Zhang, C., Tang, J., 2022. Experimental study of coal flow characteristics under mining disturbance in China. Int. J. Coal Sci. Technol. 9, 66.
Zhang, X., Jin, C., Zhang, D., Zhang, C., Ranjith, P.G., Yuan, Y., 2023. Carbon dioxide flow behaviour in macro-scale bituminous coal: an experimental determination of the influence of effective stress. Energy 268, 126754.
Zou, G., Zhang, Q., Peng, S., She, J., Teng, D., Jin, C., Che, Y., 2022. Influence of geological factors on coal permeability in the Sihe coal mine. Int. J. Coal Sci. Technol. 9, 6.